Multidisciplinary Output Research For Actual and International Issue (MORFAI Journal) ISSN (e): 2808-6635
Volume 6 No. 5 (2026)

MULTI-OBJECTIVE OPTIMIZATION OF TAF VENTILATION SYSTEMS WITH DIFFERENT INLET GEOMETRIES FOR PARTICLE CONTROL AND THERMAL COMFORT IN OPERATING ROOMS

Ghiffar Yanuar*, Sholahudin, Kurniawan Teguh. Waskito, Ridho Irwansyah
Department of Mechanical Engineering, Faculty of Engineering, Universitas Indonesia, Depok, West Java, Indonesia. HP. 085290842166
*E-mail: ghiffar.yanuar@ui.ac.id

Received	: 01 June 2026	Accepted	: 15 June 2026
Revised	: 05 June 2026	Published	: 19 July 2026

Abstract

Operating room ventilation plays an important role in controlling bacteria-carrying particles (BCP), reducing infection risk, and maintaining thermal comfort for medical staff. Temperature-controlled airflow (TAF) is a promising ventilation strategy because it supplies air through central and peripheral inlets with different temperatures to form a stable downward airflow. This study aims to optimize a TAF ventilation system by considering BCP concentration, energy consumption, and predicted mean vote (PMV). A three-dimensional operating room model was developed using computational fluid dynamics (CFD). Four operating parameters were varied using central composite design (CCD), while the peripheral inlet position was evaluated separately as a two-level geometry parameter. Airflow was solved using the RNG k–ε turbulence model, while BCP motion was modeled using the discrete phase model (DPM). CFD simulation results were used to train an artificial neural network (ANN) model, which was then integrated with a multi-objective genetic algorithm (MOGA). TOPSIS was used to select the best compromise solution from the Pareto front. The optimum condition was obtained at a central inlet velocity of 0.2735 m/s, peripheral inlet velocity of 0.1671 m/s, central inlet temperature of 21.8649 °C, peripheral inlet temperature of 22.0127 °C, and peripheral-to-central inlet distance of 2.0474 m. This configuration produced a BCP concentration of 0.9115 CFU/m³, energy consumption of 9.8832 kW, and PMV of −0.3186. These results indicate that the modified TAF configuration can produce low particle concentration, relatively low energy consumption, and acceptable thermal comfort in the operating room.

Keywords: Temperature-controlled airflow, Operating room Bacteria-Carrying Particles, Energy Consumption, Predicted Mean Vote, Multi-objective optimization

1. INTRODUCTION

Operating room air quality is an important factor in reducing the risk of surgical site infection caused by airborne contamination. Bioaerosols and particulates in operating rooms have been reported to contribute to an increased risk of postoperative infection (He et al., 2017; Humbal et al., 2018). One of the main contaminants is bacteria-carrying particles (BCP), which can be released by medical staff through breathing, skin particle shedding, body movement, and interaction with surgical equipment (Buonanno et al., 2019; Hoffman et al., 2002). These particles can be transported by indoor airflow and accumulate around the surgical zone when the ventilation system is not properly designed. Therefore, effective ventilation is required to control particle dispersion, maintain sterile conditions, and support thermal comfort during surgical procedures (Buonanno et al., 2019; He et al., 2017; Humbal et al., 2018).

Several ventilation strategies have been applied in operating rooms, including turbulent mixing airflow (TMA), laminar airflow (LAF), and temperature-controlled airflow (TAF), each of which has its own advantages and limitations (Arison et al., 2025). TMA works through a dilution mechanism, but turbulent mixing can create recirculation zones that transport particles back to the surgical area (Sadrizadeh et al., 2021). LAF can generate downward unidirectional airflow and significantly reduce particle contamination (Schumann et al., 2023; Wang et al., 2018), but its performance is sensitive to flow obstructions caused by surgical lamps, medical staff, and human thermal plumes, and it generally requires a high airflow rate that can increase energy consumption (Aganovic et al., 2017; Sadrizadeh et al., 2014; Arison et al., 2025). Compared with these systems, TAF offers a promising approach by supplying cool air through the central inlet and warmer air through the peripheral inlets to form a stable downward airflow toward the operating table (Alsved et al., 2018; Arison et al., 2025; Wang et al., 2018).

Previous studies have shown that TAF provides more stable BCP cleaning performance, is less sensitive to physical disturbances, and can maintain air quality under complex thermal load conditions (Alsved et al., 2018; Z. Liu et al., 2021; D'Alicandro & Mauro, 2023). Arison et al. (2025) optimized a TAF system using computational fluid dynamics (CFD), central composite design (CCD), artificial neural network (ANN), and multi-objective optimization to minimize BCP and energy consumption, and demonstrated a trade-off between air quality and energy efficiency through Pareto solutions (Arison et al., 2025; Melanie, 1999). However, thermal comfort assessment using predicted mean vote (PMV) has not been included as a performance indicator, although medical staff may experience thermal discomfort due to low supply temperature, high local air velocity, and the use of protective clothing (D'Alicandro & Mauro, 2023; Massarotti et al., 2021).

In addition to thermal comfort, inlet geometry also plays an important role in operating room ventilation performance. The size, position, and arrangement of diffusers affect airflow distribution, turbulence intensity, particle transport, and temperature fields (Aganovic et al., 2017; Z. Liu, Yin, Niu, et al., 2022; Sadrizadeh et al., 2014). The interaction among diffuser outlet velocity, surgical lamps, and human thermal plumes can also influence ultra-clean ventilation performance and BCP dispersion in the operating room microenvironment (Chow et al., 2006; Z. Liu, Yin, Niu, et al., 2022; Sadrizadeh et al., 2014). Therefore, inlet geometry modification, particularly the position of the peripheral inlets relative to the central inlet, needs to be investigated to obtain a better balance among air cleanliness, energy efficiency, and thermal comfort.

CFD is widely used in operating room ventilation studies because it can predict airflow patterns, temperature distribution, turbulence characteristics, and particle dispersion in detail (Chen et al., 2006; D'Alicandro & Mauro, 2023). In this study, CFD was used to evaluate a modified TAF system with two peripheral inlet positions. The simulation results were used to build an ANN as a surrogate model that represents the nonlinear relationship between input parameters and output responses, including BCP, energy consumption, and PMV (K. Li et al., 2013; Mohanraj et al., 2012; Nasruddin et al., 2019). Furthermore, a multi-objective genetic algorithm (MOGA) was used to determine the optimum configuration, while TOPSIS was applied to select the best compromise solution from the Pareto front (Melanie, 1999).

Based on this background, this study aims to optimize a modified TAF ventilation system in an operating room by simultaneously considering BCP, energy consumption, and PMV as representations of air cleanliness, energy efficiency, and thermal comfort (Chen et al., 2006; D'Alicandro & Mauro, 2023; Melanie, 1999). The operating parameters were varied using CCD, while the peripheral inlet position was evaluated as a two-level geometry parameter. The novelty of this study lies in the integration of inlet geometry modification and PMV evaluation within a CFD–ANN–MOGA optimization framework, which has not been widely discussed in previous TAF studies (Arison et al., 2025; Nasruddin et al., 2019). The results are expected to provide design recommendations for an operating room ventilation system that is clean, energy-efficient, and thermally acceptable for medical staff.

2. RESEARCH METHODS

2.1 Research framework

This study employed a numerical and optimization-based approach to evaluate the performance of a modified temperature-controlled airflow (TAF) ventilation system in an operating room. The research framework consisted of computational fluid dynamics (CFD) simulation, artificial neural network (ANN) modeling, multi-objective genetic algorithm (MOGA) optimization, and solution selection using the technique for order preference by similarity to ideal solution (TOPSIS). The CFD model was used to calculate airflow distribution, bacteria-carrying particle (BCP) concentration, energy consumption, and predicted mean vote (PMV). The simulation results were then used as training data for the ANN model. The trained ANN model was applied as a surrogate model in the MOGA optimization process. Finally, TOPSIS was used to select the best compromise solution from the Pareto front.

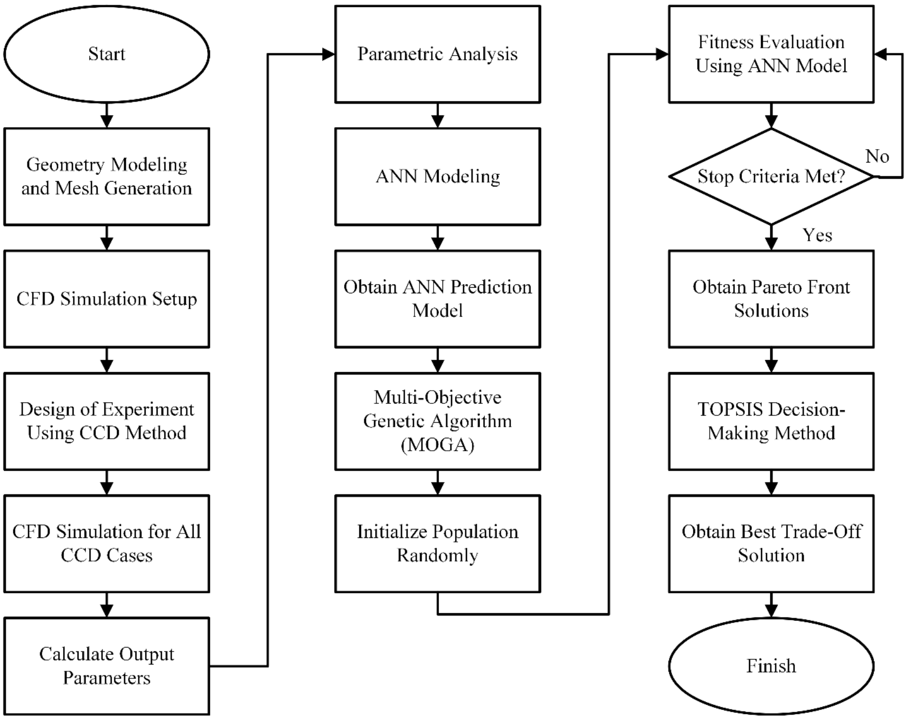

Figure 1. CFD–ANN–MOGA–TOPSIS optimization research framework

2.2 Operating room geometry and inlet configuration

The operating room model was developed based on a standard configuration used in previous ventilation studies (Arison et al., 2025). The room measured 6 m × 6 m × 3 m and was equipped with one central inlet diffuser (2 m × 2 m above the operating table), eight peripheral inlet diffusers (0.54 m × 0.54 m, with 0.06 m spacing), eight outlets (0.98 m × 0.28 m, installed on the lower wall 0.21 m above the floor), two surgical lamps, one operating table, one patient, and four medical staff. The operating table was placed at the center of the room with dimensions of 1.8 m × 0.5 m × 0.77 m. The patient was assumed to be stationary and covered, and therefore was not modeled as a heat or BCP source (Z. Liu, Yin, Hu, et al., 2022). The two surgical lamps were modeled as heat sources and flow obstructions, with glass and cover temperatures of 27.5 °C and 29.2 °C, respectively (Massarotti et al., 2021).

Two inlet configurations were evaluated based on the distance between the central inlet and the peripheral inlet, namely 1.38 m for Geometry 1 and 2.08 m for Geometry 2, as shown in Figure 2. This variation was used to investigate the influence of peripheral inlet position on airflow distribution, BCP dispersion, energy consumption, and thermal comfort. The central inlet was designed to supply cool air directly toward the operating table, while the peripheral inlets supplied air around the central zone to support stable vertical airflow in the TAF system. In the simulation, the central and peripheral inlets were set as velocity inlets with velocity ranges of 0.20–0.28 m/s and 0.14–0.20 m/s, respectively, while the outlets were set as pressure outlets with a gauge pressure of 0 Pa. Each medical staff member was modeled with a height of 1.67 m, a body surface area of 1.51 m², a heat flux of 116 W/m², and a BCP emission source of 600 CFU/min with a particle diameter of 12 µm and a density of 1000 kg/m³ (Arison et al., 2025; Sadrizadeh et al., 2014; J. Liu et al., 2009; Rui et al., 2008; Wang et al., 2018).

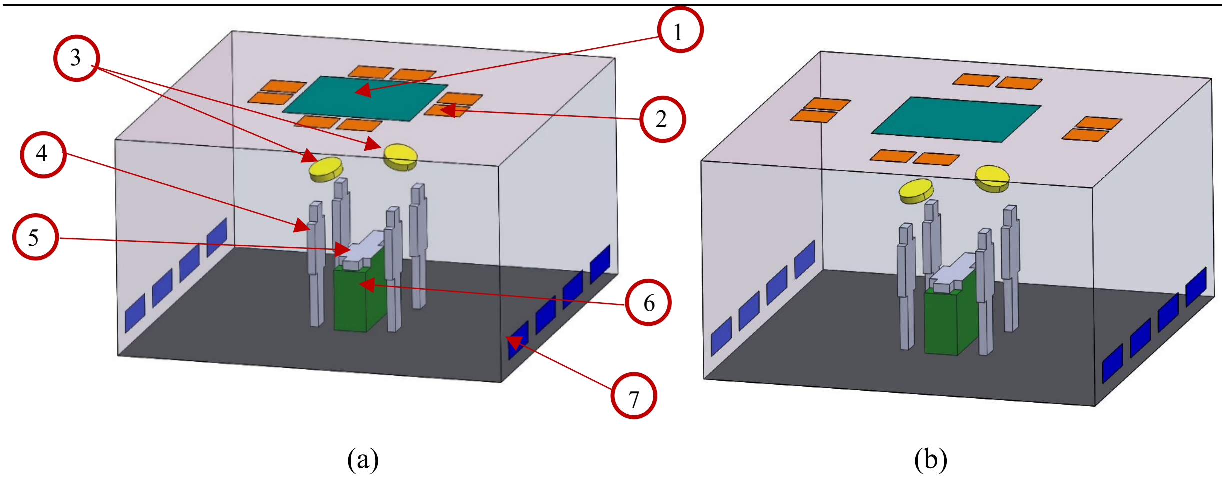

Figure 2. Operating room model with modified geometry: (a) Geometry 1, (b) Geometry 2; (1) central inlet diffuser, (2) peripheral inlet diffuser, (3) surgical lamp, (4) medical staff, (5) patient, (6) operating table, and (7) outlet diffuser.

To evaluate ventilation performance in the critical area, data were collected around the operating table using 16 sampling points labeled P1–P16, which were arranged symmetrically above the operating table at various horizontal and vertical positions, as shown in Figure 3. These points represent the patient area and the working zone of medical staff, and were used to obtain BCP concentration and local air parameters required for PMV calculation. Data from all sampling points were then averaged to evaluate the TAF system performance specifically in the operating zone, so that the assessment reflected the air quality and thermal comfort conditions in the surgical area rather than only the whole-room average.

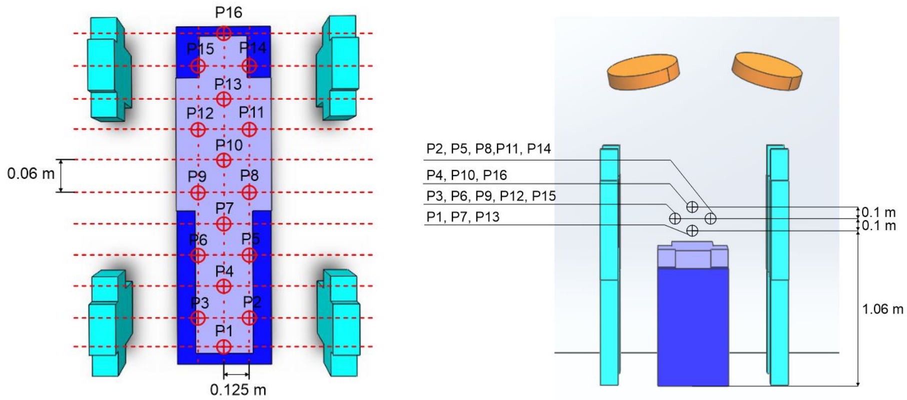

Figure 3. Top and side views of the sampling point locations

2.3 Mathematical model for numerical simulation

The mathematical model in this study was developed to represent the three main phenomena in the operating room. All mathematical formulations followed approaches used in previous operating room CFD studies and the basic formulations implemented in ANSYS Fluent.

2.3.1 Airflow phase simulation

The airflow simulation was solved using the incompressible Navier–Stokes equations within the Reynolds-Averaged Navier–Stokes (RANS) framework. For turbulence modeling, the RNG k–ε model was used because it has been recommended in previous studies for its ability to capture specific turbulence characteristics in indoor airflow (Kuznik et al., 2007; Srebric et al., 2008; Van Maele & Merci, 2006). The general RANS equation for the transport variable φ is expressed as:

$$\frac{\partial(\rho\phi)}{\partial t} + \nabla\cdot(\rho\phi\vec{V}) = \nabla\cdot(\Gamma_\phi\nabla\phi) + S_\phi \quad (1)$$

where ρ is the air density, φ is the velocity component, $\vec{V}$ is the velocity vector, Γφ is the turbulent diffusion coefficient, and Sφ is the mass or momentum source term. For the numerical scheme, SIMPLE was used for pressure–velocity coupling, PRESTO! for pressure discretization, and a second-order upwind scheme for momentum, as applied in previous operating room studies (D'Alicandro et al., 2021). Buoyancy effects were modeled using the

Boussinesq approximation, while wall boundaries were assigned no-slip conditions following the reference study (Chow et al., 2006).

2.3.2 BCP particle transport

BCP transport was modeled using the Lagrangian Particle Tracking (LPT) approach with the Discrete Random Walk (DRW) model to represent turbulent particle dispersion, as used in the reference operating room study (Wang et al., 2021). Particle motion is governed by the following equation:

$$\frac{d\overrightarrow{u_p}}{dt} = F_D(\vec{u} - \overrightarrow{u_p}) + \frac{\vec{g}(\rho_p - \rho)}{\rho_p} + \vec{F} \tag{2}$$

The LPT–DRW model considered the relevant forces according to the reference. In the equation, $\vec{u}$ and $\overrightarrow{u_p}$ denote the fluid and particle velocities, respectively, ρ and ρ_p are the fluid and particle densities, and $\vec{F}$ represents the additional force term following Wang et al. (2021). BCP concentration was expressed as colony forming units (CFU) throughout the domain, while total particle concentration was calculated from the accumulated particles passing through each cell (DPM concentration), according to the procedure of Wang et al. (2021).

2.3.3 Energy consumption

The calculation of energy consumption in the ventilation system followed the approach used in previous studies (K. Li et al., 2013; N. Li et al., 2019; Zhou & Haghighat, 2009). The total energy consisted of fan energy and the energy required for heating or cooling the supplied air. The total energy is expressed as:

$$E_{total} = E_{fan} + E_{cooling/heating} \tag{3}$$

$$E_{fan} = \frac{PV_{air}}{\eta_{fan}} \tag{4}$$

The fan data were based on the ZIEHL-ABEGG Vpro-RH50V-ZIK GG.1R model, which operates at 380–400 V and 50/60 Hz and has an efficiency of 66.5% according to the manufacturer performance curve. The values of P and V_{air} were obtained from the inlet condition variation in each simulation scenario. In addition to fan energy, air-conditioning energy was calculated based on the temperature and enthalpy differences between return air, supply air, and outdoor air:

$$E_{cooling/heating} = \dot{m}_{supply} C_p (T_{return} - T_{supply}) + \dot{m}_{outdoor}(h_{outdoor} - h_{return}) \tag{5}$$

The thermophysical properties of air followed reference values, namely a density of 1.205 kg/m³, specific heat capacity of 1005 J/kg·°C, and outdoor relative humidity of 50%, with an outdoor temperature of 33 °C assumed according to the Jakarta climate (Standar Nasional Indonesia Konservasi Energi Sistem Tata Udara Pada Bangunan Gedung, 2020; Ventilation of Health Care Facilities, 2020). Variations in inlet velocity and supply temperature resulted in different energy consumption values for each scenario.

2.3.4 PMV calculation

At this stage, CFD simulation results in the form of air temperature distribution (t_a), mean radiant temperature (t_r), and air velocity (u) were used together with relative humidity, metabolic rate, and clothing insulation as inputs for PMV calculation. PMV was calculated according to ISO 7730 (2005) and the approach used in previous research (D'Alicandro & Mauro, 2023). PMV describes the average human thermal sensation on a scale from −3 (cold) to +3 (hot), with 0 indicating a neutral condition. The calculation is based on the human heat balance, as defined in the following equation (D'Alicandro & Mauro, 2023):

$$PMV = (0.303e^{-0.036M} + 0.028) \left\{ \begin{array}{c} (M - W) - 3.05 \times 10^{-3}[5733 - 6.99(M - W) - p_a] - 0.42 \cdot \\ [(M - W) - 58.15] \\ -1.7 \times 10^{-5} M(5867 - p_a) \\ -0.0014M(34 - t_a) - 3.96 \times 10^{-8} \\ \cdot f_{cl} \cdot (t_{cl} + 273)^4 - (t_r + 273)^4] - f_{cl}.h_c(t_{cl} - t_a) \end{array} \right\} \tag{6}$$

where M is the metabolic rate, W is the external mechanical work, p_a is the partial water vapor pressure, ta is the air temperature, tr is the mean radiant temperature, tcl is the clothing surface temperature, f_{cl} is the clothing area factor, and h_c is the convective heat transfer coefficient. Supporting parameters such as t_{cl}, f_{cl}, and h_c were calculated according to the ISO 7730 procedure.

2.4 Model validation

Numerical model validation was conducted to ensure that the CFD settings could accurately represent airflow and particle transport phenomena before being applied to the main operating room model. The validation referred to a benchmark study of particle transport in a controlled chamber (Chen et al., 2006). The validation model was a rectangular chamber measuring 0.8 m × 0.4 m × 0.4 m, with an inlet at the upper left side and an outlet at the lower right side. Air entered through the inlet at a velocity of 0.225 m/s along the x-axis. The simulation used the RNG k–ε turbulence model under steady incompressible flow assumptions, while particle transport was analyzed using the discrete phase model (DPM) with particles of 10 μm diameter and 1400 kg/m³ density according to the benchmark configuration. The validation results were compared with experimental and numerical data from the reference using x-direction velocity profiles and normalized particle concentrations. Data were sampled along three vertical lines at x = 0.2 m, x = 0.4 m, and x = 0.6 m, where the velocity profile comparison is shown in Figure 5(a) and the normalized particle concentration comparison in Figure 5(b).

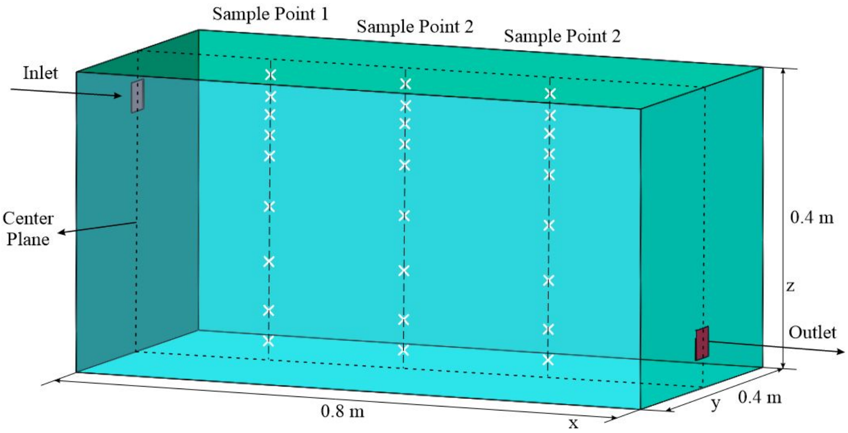

Figure 4. Validation model geometry

Based on Figure 5(a), the simulated x-direction velocity profiles show trends similar to the experimental and numerical benchmark data at the three observation positions. In Figure 5(b), the normalized particle concentration distribution also follows the reference data pattern, although slight deviations appear at several points. These deviations may be caused by the sensitivity of the turbulence model, local recirculation effects, and differences in numerical approaches for particle dispersion modeling. Overall, the validation results demonstrate good agreement with the benchmark data, indicating that the CFD settings used in this study are sufficiently valid for simulating airflow and BCP transport in the operating room.

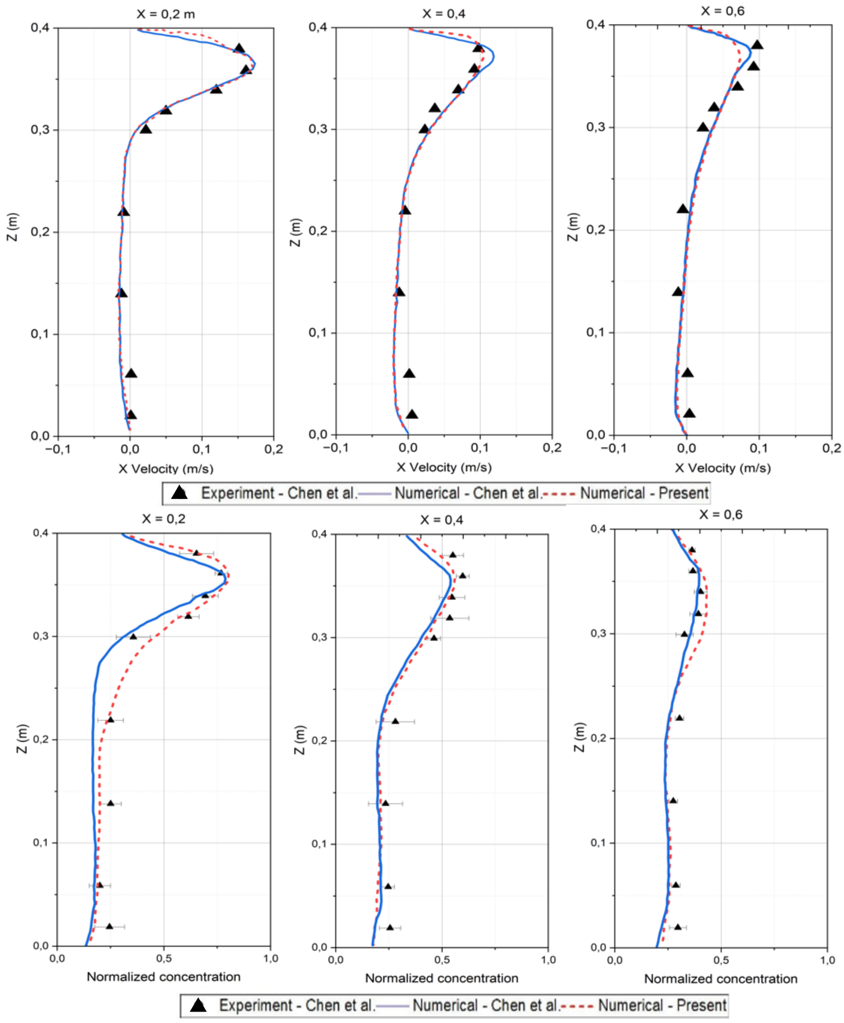

Figure 5. Validation results comparison: (a) x-direction velocity and (b) normalized particle concentration

2.5 Grid independence test

A grid independence test was performed to ensure that the CFD results were not significantly affected by mesh density. Three mesh resolutions were evaluated, namely coarse, medium, and fine meshes. The coarse mesh consisted of 2,037,433 cells, the medium mesh consisted of 2,351,750 cells, and the fine mesh consisted of 3,464,038 cells. The velocity distribution along the Z-line inside the operating room, as shown in Figure 6(a), was used as the comparison parameter.

The comparison shows that the medium and fine meshes produce similar velocity distribution patterns along most of the Z-line, as shown in Figure 6(b). The coarse mesh shows larger deviations, particularly in regions with high velocity gradients and local turbulence. Quantitatively, the normalized root mean square error between the medium and fine meshes is approximately 2.06%, while the error between the coarse and fine meshes is approximately 10.13%. The average percentage difference between the medium and fine meshes is approximately 4.34% and decreases to approximately 3.73% after filtering regions with extreme local fluctuations. Based on these results, the medium mesh was selected for all main simulations because it provides a good balance between numerical accuracy and computational efficiency.

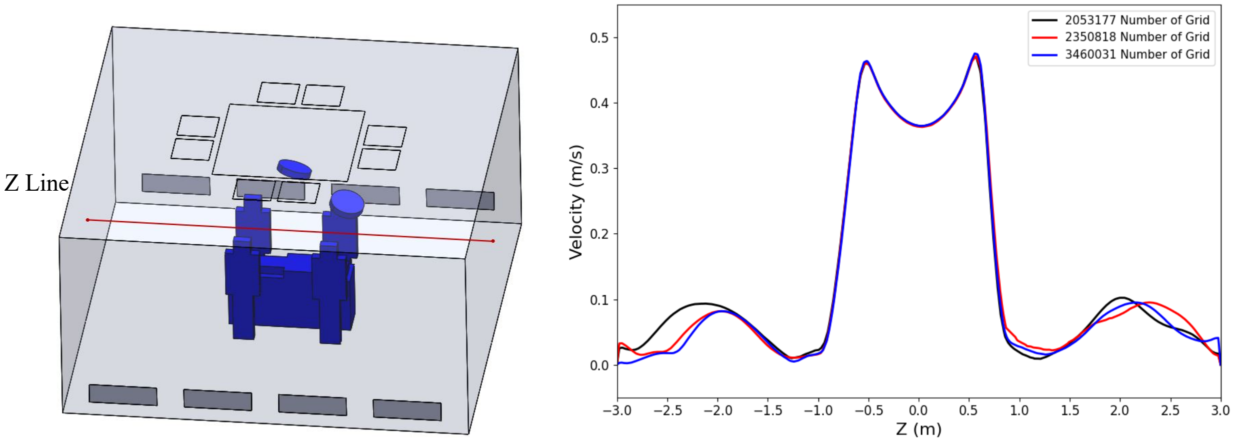

(a) (b)

Figure 6. (a) Z-line position for the grid independence test and (b) velocity comparison along the Z-line for coarse, medium, and fine meshes

2.6 Experimental design

The experimental design was developed using the Box–Wilson central composite design (CCD) method to evaluate nonlinear effects and interactions among operating parameters with a more efficient number of simulations than a full factorial design. This study used a face-centered CCD with an alpha value of 1, so that factorial and axial points were located at the same distance from the design center point (Bevilacqua et al., 2010; Bhattacharya, 2021). Four operating parameters were varied in the CCD, namely central inlet velocity of 0.20–0.28 m/s, peripheral inlet velocity of 0.14–0.20 m/s, central inlet temperature of 18–22 °C, and peripheral inlet temperature of 22–24 °C. The center point was set at a central inlet velocity of 0.24 m/s, peripheral inlet velocity of 0.17 m/s, central inlet temperature of 20 °C, and peripheral inlet temperature of 23 °C.

In addition to the operating parameters, this study also evaluated the effect of peripheral inlet position as a two-level geometry parameter. The peripheral inlet position was not included as a CCD factor because it was not treated as a continuous operating variable. Geometry 1 used a peripheral-to-central inlet distance of 1.38 m, while Geometry 2 used a distance of 2.08 m. Thus, 25 CCD runs were applied to both inlet geometries, resulting in a total of 50 CFD simulation cases. The CCD matrix used is summarized in Table 1, with each run simulated for Geometry 1 and Geometry 2 to evaluate the influence of peripheral inlet position on BCP concentration, energy consumption, and PMV.

Table 1. Factors and variable levels in the CCD design

Factor	Symbol	-1	0	+1	Unit
Central inlet velocity	A	0,20	0,24	0,28	m/s
Peripheral inlet velocity	B	0,14	0,17	0,20	m/s
Central inlet temperature	C	18	20	22	°C
Peripheral inlet temperature	D	22	23	24	°C

Based on the factor levels in Table 1, the face-centered CCD generated 25 run combinations consisting of factorial points, axial points, and center points. Each run combination was then applied to two inlet geometry configurations, namely Geometry 1 with a peripheral-to-central inlet distance of 1.38 m and Geometry 2 with a distance of 2.08 m. Therefore, the total number of CFD simulation cases in this study was 50. The complete CCD matrix is not displayed for presentation efficiency; however, all simulation combinations were developed based on the factor levels shown in Table 1.

2.7 Model ANN

Artificial neural network (ANN) was used to model the nonlinear relationship between input variables and output responses in the modified TAF ventilation system. ANN served as a surrogate model to predict BCP concentration, energy consumption, and PMV based on CFD simulation data, allowing the optimization process to be conducted without repeatedly running CFD simulations (Nasruddin et al., 2019).

The ANN model used was a multilayer perceptron (MLP) with a feed-forward configuration. The training data consisted of 50 datasets obtained from CFD simulations. The input variables included central inlet velocity, peripheral inlet velocity, central inlet temperature, peripheral inlet temperature, and the distance between the central and peripheral inlets. The distance parameter represented the two inlet geometry configurations, namely 1.38 m for

Geometry 1 and 2.08 m for Geometry 2. Meanwhile, the output variables consisted of BCP concentration, energy consumption, and PMV.

ANN training was performed using the Bayesian Regularization Backpropagation algorithm (trainbr) because it has good generalization capability for limited datasets and can reduce the risk of overfitting (Nasruddin et al., 2019). The output layer used a linear transfer function because the predicted responses were continuous variables. The ANN architecture was determined through a trial-and-error method by varying the number of neurons in the hidden layer. Model performance was evaluated using the root mean square error (RMSE), expressed as:

$$RMSE = \sqrt{\frac{1}{n}\sum_{i=1}^{n}(y_i - \hat{y}_i)^2} \tag{7}$$

where yi is the CFD simulation result, ŷi is the ANN prediction, and n is the number of data points. Based on the RMSE evaluation, the best architecture was obtained with 21 neurons in the hidden layer, with a minimum RMSE value of 0.134. The trained ANN model was then used in the multi-objective optimization process to explore combinations of operating and geometry parameters more efficiently.

The final ANN structure used in this study consisted of five input neurons, one hidden layer, and three output neurons, as shown in Figure 7. The five input neurons represented central inlet velocity, peripheral inlet velocity, central inlet temperature, peripheral inlet temperature, and the peripheral-to-central inlet distance. The three output neurons represented BCP concentration, energy consumption, and PMV. The trained ANN model was then used as a surrogate model in the multi-objective optimization process, enabling rapid performance prediction without repeatedly running CFD simulations.

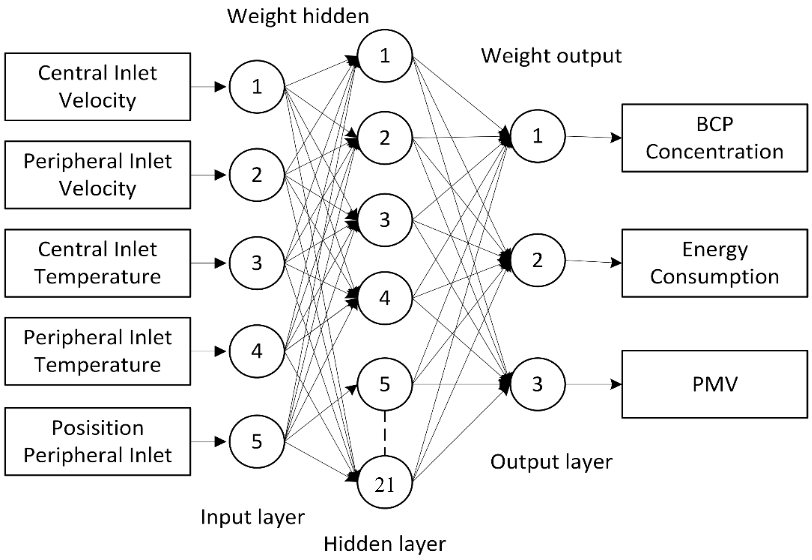

Figure 7. Artificial neural network structure

2.8 Multi-objective optimization and TOPSIS selection

The optimization procedure in this study was performed by integrating the trained ANN model with a multi-objective genetic algorithm (MOGA). MOGA is an evolutionary optimization method suitable for solving nonlinear problems with more than one objective because it searches for a set of non-dominated solutions rather than a single solution (Melanie, 1999). In this study, the ANN model was used as a surrogate model to predict system responses for new combinations of input variables without repeatedly running CFD simulations. The decision variables consisted of five parameters, namely central inlet velocity, peripheral inlet velocity, central inlet temperature, peripheral inlet temperature, and the distance between the central and peripheral inlets. These variables are expressed as:

$$x = [v_c, v_p, T_c, T_p, d] \tag{8}$$

where vc is the central inlet velocity, vp is the peripheral inlet velocity, Tc is the central inlet temperature, Tp is the peripheral inlet temperature, and d is the distance between the central and peripheral inlets. The objective functions were formulated to minimize BCP concentration, minimize energy consumption, and maintain PMV close to the neutral thermal sensation. Therefore, the multi-objective optimization problem is expressed as:

$$\min\ f(x) = [BCP(x), E(x), |\ PMV(x)\ |] \tag{9}$$

where BCP(x) is the predicted BCP concentration, E(x) is the predicted energy consumption, and |PMV(x)| is the absolute PMV value relative to the neutral condition. The use of |PMV| is required to direct the optimization toward a thermal condition close to neutral, rather than selecting a numerically smaller negative PMV value that may represent an excessively cold sensation. The MOGA process was carried out through initial population generation, objective function evaluation using the ANN model, and population updating through selection, crossover, and mutation until the stopping criteria were met. The final output was a Pareto front, which is a set of compromise solutions where improvement in one objective may decrease the performance of another objective. Since the Pareto front contains several optimum alternatives, TOPSIS was used to determine the best compromise solution based on the distance of each alternative to the positive and negative ideal solutions (Shih et al., 2007). Thus, TOPSIS enables one final optimum configuration to be selected from the Pareto front by simultaneously considering BCP concentration, energy consumption, and PMV.

3. RESULTS AND DISCUSSION

3.1 Airflow pattern and BCP distribution characteristics

Airflow pattern analysis was conducted to evaluate the effects of central inlet velocity and peripheral inlet position on the formation of downward airflow in the TAF system. This airflow pattern is important because clean air from the central diffuser must move stably toward the operating table to help reduce BCP accumulation in the surgical zone.

Based on Figure 8(a)–(d), increasing the central inlet velocity from 0.20 to 0.28 m/s strengthens the downward air jet toward the operating area. At low velocity, the airflow in the central zone tends to be weaker and is more easily affected by recirculation around operating room objects. In contrast, at high velocity, the airflow momentum increases, making the downward airflow clearer and better able to reach the operating table.

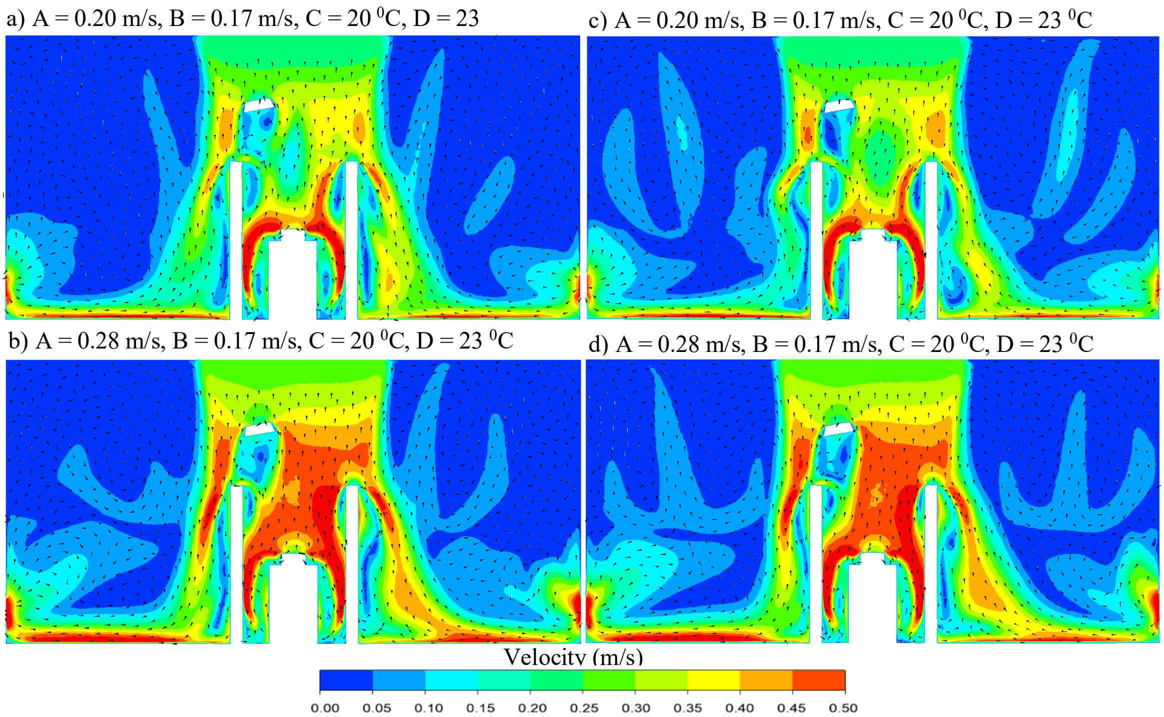

Figure 8. Effect of central inlet velocity on airflow pattern for Geometry 1 (a and b) and Geometry 2 (c and d)

Figure 9(a)–(d) shows that the central inlet temperature also affects the airflow structure. At a low temperature of 18 °C, the cooler supply air has a higher density, making the downward motion more dominant due to the buoyancy effect. Conversely, when the central inlet temperature increases to 22 °C, the temperature difference between the supply air and the surrounding air decreases, weakening the buoyancy effect and making the downward airflow pattern less uniform. Overall, the visualization indicates that central inlet velocity strengthens the vertical jet momentum, while central inlet temperature affects airflow stability through the buoyancy effect.

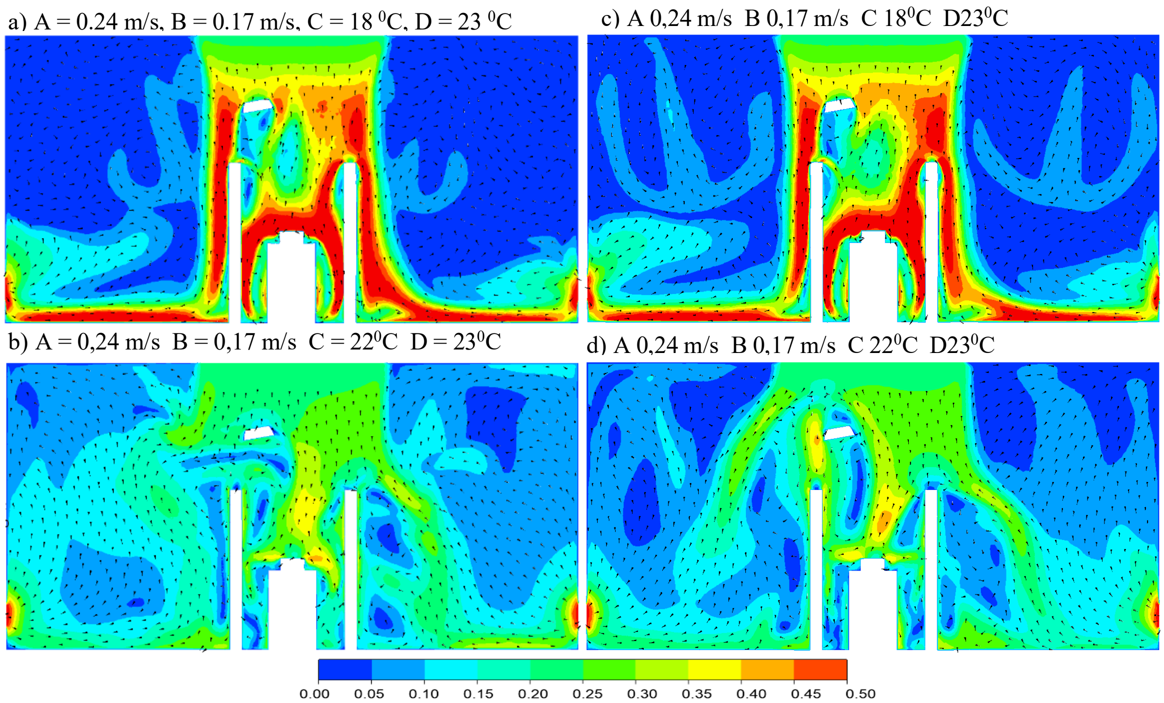

Figure 9. Effect of central inlet temperature on airflow pattern for Geometry 1 (a and b) and Geometry 2 (c and d)

The effect of central inlet velocity on BCP distribution is shown in Figure 10. At low velocity, BCP concentration is still observed around the medical staff bodies and the lower part of the operating zone because the downward airflow momentum is not strong enough to carry particles away from their sources. When the central inlet velocity increases to 0.28 m/s, the BCP distribution appears slightly more localized around the particle sources and side areas, so accumulation in the central zone tends to decrease. However, the visual difference between low and high velocities is not very significant because BCP distribution is also influenced by local recirculation, thermal plume, surgical lamp obstruction, and the interaction between central and peripheral airflow.

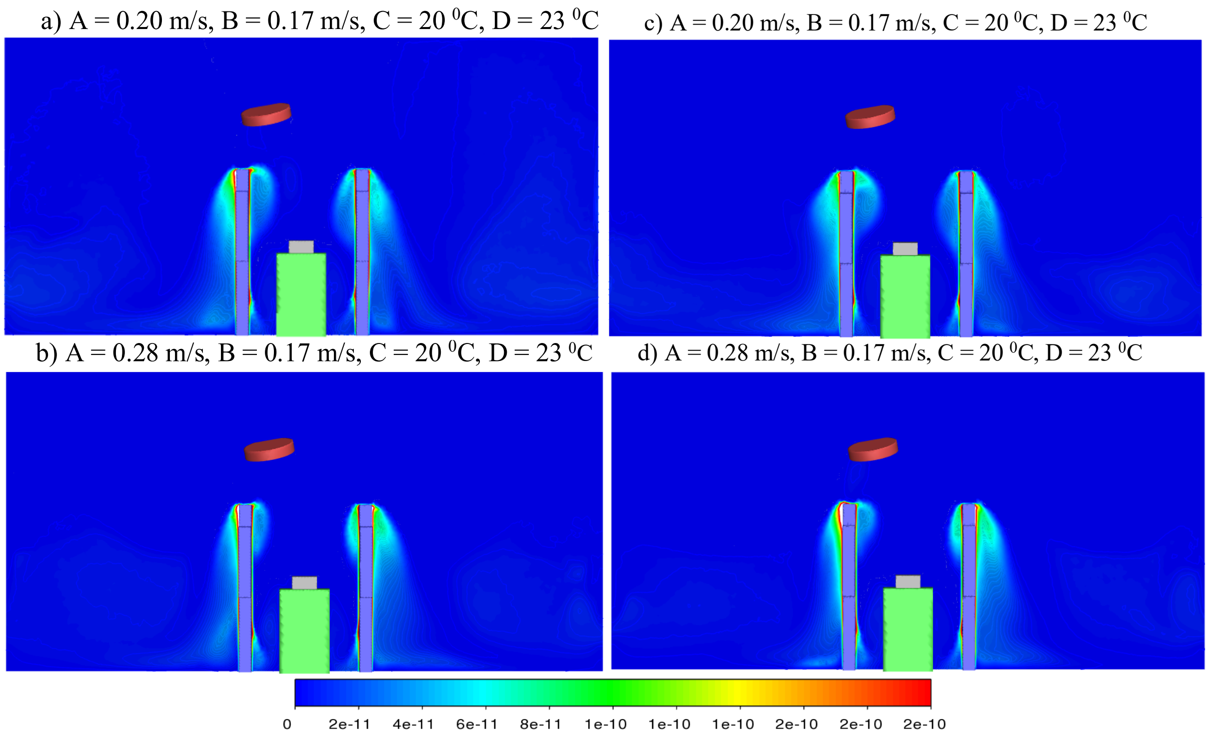

Figure 10. BCP particle concentration distribution on a vertical plane for central inlet velocity variation in Geometry 1 (a and b) and Geometry 2 (c and d)

Figure 11 shows the effect of central inlet temperature on BCP distribution in Geometry 1 and Geometry 2. At lower central inlet temperature, the cooler supply air has a higher density, so the buoyancy effect strengthens the downward air motion. This condition helps carry particles downward and limits their dispersion around the surgical zone. Conversely, when the central inlet temperature increases, the temperature difference between supply air and surrounding air becomes smaller, weakening the downward airflow and making BCP dispersion easier. Therefore, central inlet temperature plays an important role in maintaining downward airflow stability and supporting particle removal from the critical zone.

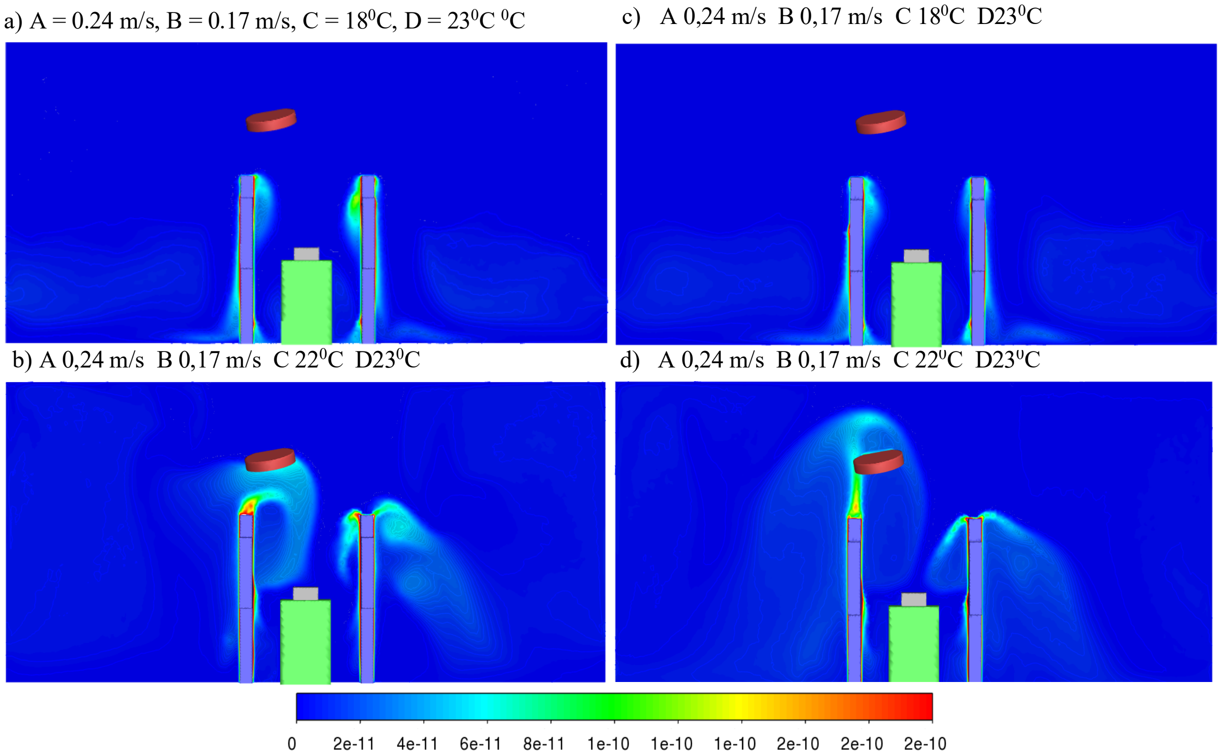

Figure 11. BCP particle concentration distribution on a vertical plane for central inlet temperature variation in Geometry 1 (a and b) and Geometry 2 (c and d)

The comparison between Geometry 1 and Geometry 2 indicates that the peripheral inlet position also affects the BCP transport pattern under temperature variation. In both geometries, lower central inlet temperature produces a more localized particle distribution, whereas higher central inlet temperature causes a wider dispersion pattern. Nevertheless, the spatial particle trajectories differ depending on the peripheral inlet arrangement, indicating that the interaction between thermal buoyancy and side airflow also influences particle paths around the surgical zone. Thus, temperature variation demonstrates that central inlet temperature strongly affects BCP dispersion through its influence on airflow stability and buoyancy effects. Lower central inlet temperature tends to increase particle localization around the sources, whereas higher central inlet temperature increases the possibility of wider particle dispersion within the operating room.

3.2 Parametric analysis of BCP concentration, energy consumption, and PMV

Parametric analysis was performed to evaluate the effect of central inlet velocity on BCP concentration, energy consumption, and PMV. In this case, the central inlet velocity was varied from 0.20 to 0.28 m/s, while peripheral inlet velocity, central inlet temperature, and peripheral inlet temperature were kept constant at 0.17 m/s, 20 °C, and 23 °C, respectively. Figure 12 shows that increasing the central inlet velocity generally reduces BCP concentration, particularly in Geometry 2. This indicates that higher inlet velocity strengthens downward airflow and enhances particle removal from the operating zone. However, the decrease in BCP is accompanied by an increase in energy consumption in both geometries, because higher inlet velocity requires a greater airflow rate and fan power. The PMV value also decreases as the central inlet velocity increases. This trend indicates that higher air velocity makes the thermal sensation colder due to increased convective heat transfer around the operating zone. Thus, although increasing the central inlet velocity can improve BCP removal, it also increases energy consumption and shifts PMV toward a colder sensation. This confirms that the selection of central inlet velocity must consider the balance among air cleanliness, energy efficiency, and thermal comfort.

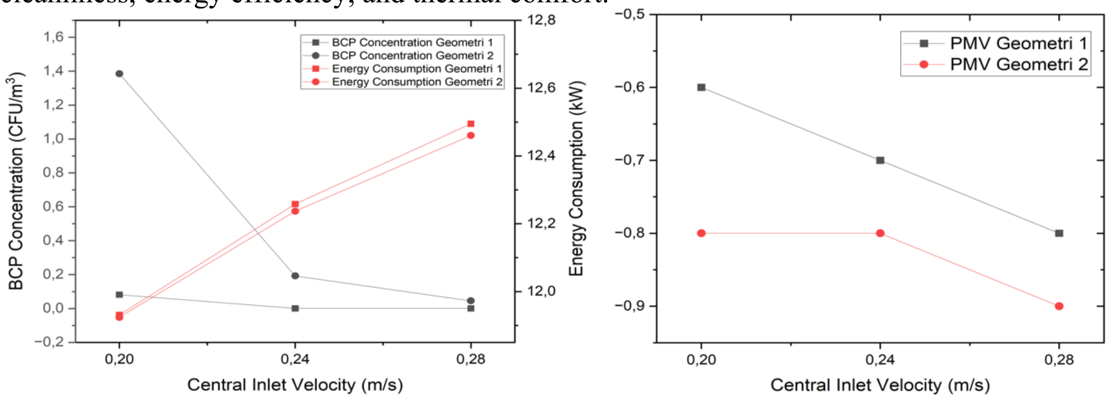

Figure 12. Effect of central inlet velocity on BCP concentration, energy consumption, and PMV.

Figure 13 shows the effect of central inlet temperature on BCP concentration, energy consumption, and PMV. Increasing the central inlet temperature from 18 °C to 22 °C tends to increase BCP concentration in both geometries, with a clearer increase in Geometry 2. This indicates that a higher supply temperature weakens downward airflow, thereby reducing the system ability to remove particles from the operating zone. Conversely, lower central inlet temperature produces cooler and denser supply air, so the buoyancy effect strengthens downward airflow and supports particle removal from the critical area.

In terms of energy consumption, increasing the central inlet temperature generally reduces energy demand because the cooling load of the ventilation system becomes smaller. The PMV value also increases with central inlet temperature, so the thermal condition shifts from a colder sensation toward a more neutral condition. Thus, central inlet temperature shows a trade-off among BCP control, energy consumption, and thermal comfort. Lower temperature supports particle removal but requires higher energy and produces colder thermal conditions. Conversely, higher temperature reduces energy consumption and brings PMV closer to neutral, but may increase BCP concentration in the operating zone.

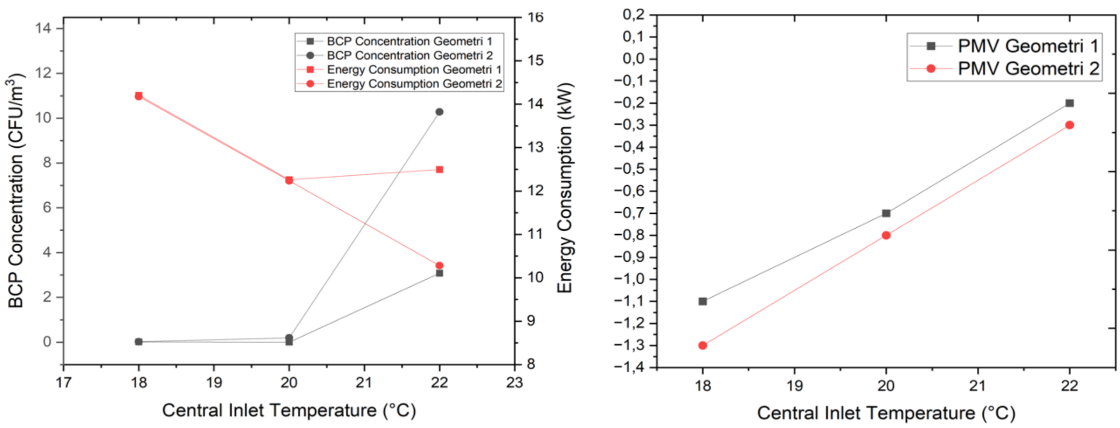

Figure 13. Effect of central inlet temperature on BCP concentration, energy consumption, and PMV.

3.3 ANN prediction performance

The ANN model performance was evaluated by comparing ANN predictions with CFD simulation data for three output responses, namely BCP concentration, energy consumption, and PMV. The evaluation was conducted using 50 simulation cases consisting of 25 CCD runs for Geometry 1 and 25 CCD runs for Geometry 2. The comparison between ANN predictions and CFD simulation data is shown in Figure 14.

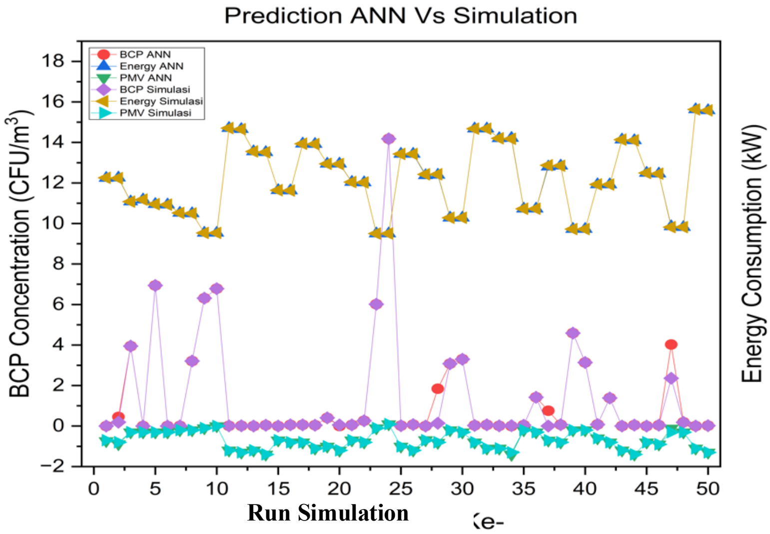

Figure 14. Comparison between ANN prediction results and CFD simulation data.

Based on Figure 14, the ANN prediction results generally follow the CFD simulation data trends for all output responses. Energy consumption prediction shows good agreement with the simulation data, as indicated by the nearly overlapping patterns between ANN and CFD results. PMV prediction also consistently follows the simulation trend, indicating that the ANN model can represent the effects of inlet velocity, inlet temperature, and geometry variation on thermal comfort.

For the BCP concentration response, several deviations still occur in certain runs, particularly when the CFD data show relatively high particle concentrations. This may occur because BCP transport is highly sensitive to local airflow behavior, recirculation, particle trajectories, and interactions with operating room objects such as medical staff and surgical lamps. Nevertheless, the ANN model is still able to capture the general trend of BCP concentration across all simulation cases. The regression evaluation also indicates a strong correlation between ANN predictions and CFD data, so the ANN model is considered suitable for use as a surrogate model in the multi-objective optimization process.

3.4 Multi-objective optimization and TOPSIS selection

Multi-objective optimization was performed using the trained ANN model as a surrogate model integrated with MOGA. The optimization objectives were to minimize BCP concentration, energy consumption, and the absolute deviation of PMV from the neutral thermal condition. The optimization results are presented as a Pareto front in Figure 15, where red points indicate non-dominated solutions and gray points indicate dominated solutions. The Pareto front distribution shows a trade-off relationship among particle control, energy consumption, and thermal comfort. Therefore, there is no single solution that can simultaneously minimize all objectives without sacrificing at least one of the others.

The star marker indicates the best compromise solution selected using TOPSIS. This solution is located in the region with low BCP concentration and low |PMV| while still maintaining relatively low energy consumption. The optimum condition was obtained at a central inlet velocity of 0.2735 m/s, peripheral inlet velocity of 0.1671 m/s, central inlet temperature of 21.8649 °C, peripheral inlet temperature of 22.0127 °C, and peripheral-to-central inlet distance of 2.0474 m. This distance is close to Geometry 2, indicating that a peripheral inlet position farther from the central inlet provides a better configuration for maintaining airflow stability and reducing disturbance to the main air jet.

Under the optimum condition, the system produced a BCP concentration of 0.9115 CFU/m³, energy consumption of 9.8832 kW, PMV of −0.3186, and TOPSIS score of 0.8785. The slightly negative PMV indicates a slightly cool thermal sensation but remains close to a comfortable or neutral condition. These results show that the ANN–MOGA–TOPSIS approach can identify the optimum TAF configuration that balances air cleanliness, energy efficiency, and thermal comfort.

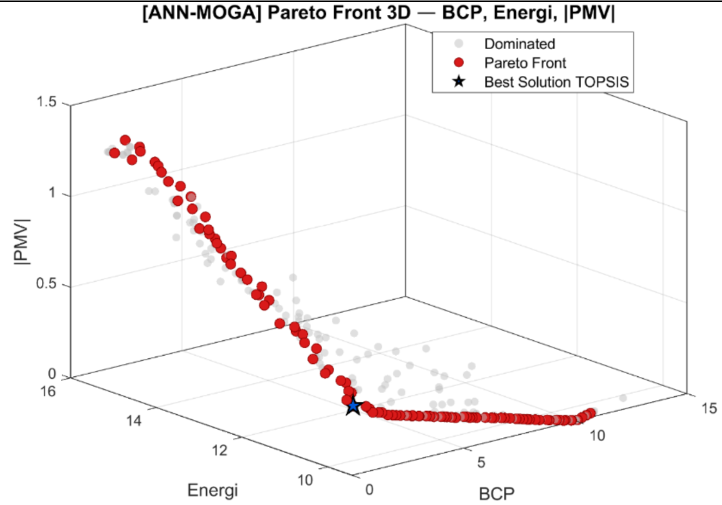

Figure 15. Three-dimensional Pareto front from ANN–MOGA optimization and optimum TOPSIS solution.

4. CONCLUSION

This study analyzed the performance of a modified temperature-controlled airflow (TAF) ventilation system in an operating room by considering BCP concentration, energy consumption, and PMV. The CFD results showed that central inlet velocity mainly affects downward airflow momentum, while central inlet temperature plays an important role in airflow stability through the buoyancy effect. Increasing central inlet velocity tends to reduce BCP concentration, but increases energy consumption and shifts PMV toward a colder sensation. Conversely, increasing central inlet temperature reduces energy consumption and brings PMV closer to neutral, but may increase BCP concentration.

The ANN model showed good predictive ability for the three output responses and was used as a surrogate model in multi-objective optimization. The ANN–MOGA optimization results produced a Pareto front showing trade-offs among particle control, energy efficiency, and thermal comfort. Based on TOPSIS selection, the optimum configuration was obtained at a central inlet velocity of 0.2735 m/s, peripheral inlet velocity of 0.1671 m/s, central inlet temperature of 21.8649 °C, peripheral inlet temperature of 22.0127 °C, and peripheral-to-central inlet distance of 2.0474 m. This configuration produced a BCP concentration of 0.9115 CFU/m^3, energy consumption of 9.8832 kW, PMV of −0.3186, and TOPSIS score of 0.8785. These results demonstrate that the CFD–ANN–MOGA–TOPSIS approach is effective for determining the optimum TAF configuration that balances air cleanliness, energy efficiency, and thermal comfort in the operating room.

ACKNOWLEDGMENTS

The authors would like to thank the Department of Mechanical Engineering, Faculty of Engineering, Universitas Indonesia, for the academic support and facilities provided during this study. The authors also appreciate all parties who provided discussions, technical assistance, and support during the development of the CFD model, ANN prediction model, and multi-objective optimization analysis.

NOMENCLATURE

ANN	: Artificial neural network
BCP	: Bacteria-carrying particles
CCD	: Central composite design
DPM	: Discrete phase model
MOGA	: Multi-objective genetic algorithm
PMV	: Predicted mean vote
TAF	: Temperature-controlled airflow
TOPSIS	: Technique for order preference by similarity to ideal solution
vc	: Central inlet velocity (m/s)
vp	: Peripheral inlet velocity (m/s)
Tc	: Central inlet temperature (°C)
Tp	: Peripheral inlet temperature (°C)
E	: Energy consumption (kW)

REFERENCES

Aganovic, A., Cao, G., Stenstad, L. I., & Skogås, J. G. (2017). Impact of surgical lights on the velocity distribution and airborne contamination level in an operating room with laminar airflow system. *Building and Environment*, *126*, 42–53. https://doi.org/10.1016/j.buildenv.2017.09.024

Alsved, M., Civilis, A., Ekolind, P., Tammelin, A., Andersson, A. E., Jakobsson, J., Svensson, T., Ramstorp, M., Sadrizadeh, S., Larsson, P. A., Bohgard, M., Šantl-Temkiv, T., & Löndahl, J. (2018). Temperature-controlled airflow ventilation in operating rooms compared with laminar airflow and turbulent mixed airflow. *Journal of Hospital Infection*, *98*(2), 181–190. https://doi.org/10.1016/j.jhin.2017.10.013

Arison, F. S., Tokumasu, T., Sholahudin, Yatim, A. S., & Nasruddin, N. (2025). Multi-Objective Optimization of TAF Systems: Enhancing Air Cleanliness and Energy Efficiency in Surgical Environments. *Building and Environment*, *279*. https://doi.org/10.1016/j.buildenv.2025.112977

Buonanno, G., Capuano, R., Cortellessa, G., & Stabile, L. (2019). Airborne particle emission rates and doses received in operating rooms from surgical smoke. *Building and Environment*, *151*, 168–174. https://doi.org/10.1016/j.buildenv.2019.01.044

Chen, F., Yu, S. C. M., & Lai, A. C. K. (2006). Modeling particle distribution and deposition in indoor environments with a new drift-flux model. *Atmospheric Environment*, *40*(2), 357–367. https://doi.org/10.1016/j.atmosenv.2005.09.044

Chow, T. T., Lin, Z., & Bai, W. (2006). The integrated effect of medical lamp position and diffuser discharge velocity on ultra-clean ventilation performance in an operating theatre. *Indoor and Built Environment*, *15*(4), 315–331. https://doi.org/10.1177/1420326X06067802

D'Alicandro, A. C., Massarotti, N., & Mauro, A. (2021). Aerosol hazards in operating rooms: A review of numerical and experimental studies. In *Journal of Aerosol Science* (Vol. 158). Elsevier Ltd. https://doi.org/10.1016/j.jaerosci.2021.105823

D'Alicandro, A. C., & Mauro, A. (2023). Air change per hour and inlet area: Effects on ultrafine particle concentration and thermal comfort in an operating room. *Journal of Aerosol Science*, *171*. https://doi.org/10.1016/j.jaerosci.2023.106183

He, C., Mackay, I. M., Ramsay, K., Liang, Z., Kidd, T., Knibbs, L. D., Johnson, G., McNeale, D., Stockwell, R., Coulthard, M. G., Long, D. A., Williams, T. J., Duchaine, C., Smith, N., Wainwright, C., & Morawska, L. (2017). Particle and bioaerosol characteristics in a paediatric intensive care unit. *Environment International*, *107*, 89–99. https://doi.org/10.1016/j.envint.2017.06.020

Hoffman, P. N., Williams, J., Stacey, A., Bennett, A. M., Ridgway, G. L., Dobson, C., Fraser, I., & Humphreys, H. (2002). Microbiological commissioning and monitoring of operating theatre suites. A report of a working party of the Hospital Infection Society. *Journal of Hospital Infection*, *52*(1), 1–28. https://doi.org/10.1053/jhin.2002.1237

Humbal, C., Gautam, S., & Trivedi, U. (2018). A review on recent progress in observations, and health effects of bioaerosols. In *Environment International* (Vol. 118, pp. 189–193). Elsevier Ltd. https://doi.org/10.1016/j.envint.2018.05.053

Kuznik, F., Rusaouën, G., & Brau, J. (2007). Experimental and numerical study of a full scale ventilated enclosure: Comparison of four two equations closure turbulence models. *Building and Environment*, *42*(3), 1043–1053. https://doi.org/10.1016/j.buildenv.2005.11.024

Li, K., Xue, W., Xu, C., & Su, H. (2013). Optimization of ventilation system operation in office environment using POD model reduction and genetic algorithm. *Energy and Buildings*, *67*, 34–43. https://doi.org/10.1016/j.enbuild.2013.07.075

Liu, J., Wang, H., & Wen, W. (2009). Numerical simulation on a horizontal airflow for airborne particles control in hospital operating room. *Building and Environment*, *44*(11), 2284–2289. https://doi.org/10.1016/j.buildenv.2009.03.019

Liu, Z., Liu, H., Yin, H., Rong, R., Cao, G., & Deng, Q. (2021). Prevention of surgical site infection under different ventilation systems in operating room environment. *Frontiers of Environmental Science and Engineering*, *15*(3). https://doi.org/10.1007/s11783-020-1327-9

Liu, Z., Yin, D., Hu, L., He, J., & Cao, G. (2022). Bacteria-carrying particles diffusion in the operating room due to the interaction between human thermal plume and ventilation systems: An experimental-numerical simulation study. *Energy and Buildings*, *270*. https://doi.org/10.1016/j.enbuild.2022.112277

Liu, Z., Yin, D., Niu, Y., Cao, G., Liu, H., & Wang, L. (2022). Effect of human thermal plume and ventilation interaction on bacteria-carrying particles diffusion in operating room microenvironment. *Energy and Buildings*, *254*. https://doi.org/10.1016/j.enbuild.2021.111573

Massarotti, N., Mauro, A., Mohamed, S., Nowak, A. J., & Sainas, D. (2021). Fluid dynamic and thermal comfort analysis in an actual operating room with unidirectional airflow system. *Building Simulation*, *14*(4), 1127–1146. https://doi.org/10.1007/s12273-020-0713-3

Melanie, M. (1999). *0−262−63185−7 (PB) 1. Genetics-Computer simulation.2. Genetics-Mathematical models*.

Mohanraj, M., Jayaraj, S., & Muraleedharan, C. (2012). Applications of artificial neural networks for refrigeration, air-conditioning and heat pump systems - A review. In *Renewable and Sustainable Energy Reviews* (Vol. 16, Number 2, pp. 1340–1358). https://doi.org/10.1016/j.rser.2011.10.015

Nasruddin, Sholahudin, Satrio, P., Mahlia, T. M. I., Giannetti, N., & Saito, K. (2019). Optimization of HVAC system energy consumption in a building using artificial neural network and multi-objective genetic algorithm. *Sustainable Energy Technologies and Assessments*, *35*, 48–57. https://doi.org/10.1016/j.seta.2019.06.002

Rui, Z., Guangbei, T., & Jihong, L. (2008). Study on biological contaminant control strategies under different ventilation models in hospital operating room. *Building and Environment*, *43*(5), 793–803. https://doi.org/10.1016/j.buildenv.2007.01.018

Sadrizadeh, S., Aganovic, A., Bogdan, A., Wang, C., Afshari, A., Hartmann, A., Croitoru, C., Khan, A., Kriegel, M., Lind, M., Liu, Z., Melikov, A., Mo, J., Rotheudt, H., Yao, R., Zhang, Y., Abouali, O., Langvatn, H., Sköldenberg, O., & Cao, G. (2021). A systematic review of operating room ventilation. In *Journal of Building Engineering* (Vol. 40). Elsevier Ltd. https://doi.org/10.1016/j.jobe.2021.102693

Sadrizadeh, S., Holmberg, S., & Tammelin, A. (2014). A numerical investigation of vertical and horizontal laminar airflow ventilation in an operating room. *Building and Environment*, *82*, 517–525. https://doi.org/10.1016/j.buildenv.2014.09.013

Schumann, L., Lange, J., Cetin, Y. E., & Kriegel, M. (2023). Experimental analysis of airborne contaminant distribution in an operating room with different ventilation schemes. *Building and Environment*, *244*. https://doi.org/10.1016/j.buildenv.2023.110783

Srebric, J., Vukovic, V., He, G., & Yang, X. (2008). CFD boundary conditions for contaminant dispersion, heat transfer and airflow simulations around human occupants in indoor environments. *Building and Environment*, *43*(3), 294–303. https://doi.org/10.1016/j.buildenv.2006.03.023

Van Maele, K., & Merci, B. (2006). Application of two buoyancy-modified k-ε turbulence models to different types of buoyant plumes. *Fire Safety Journal*, *41*(2), 122–138. https://doi.org/10.1016/j.firesaf.2005.11.003

Wang, C., Holmberg, S., & Sadrizadeh, S. (2018). Numerical study of temperature-controlled airflow in comparison with turbulent mixing and laminar airflow for operating room ventilation. *Building and Environment*, *144*, 45–56. https://doi.org/10.1016/j.buildenv.2018.08.010